Full length article

Gibbs energy and phase-field modeling of ferromagnetic ferrite (α)→ paramagnetic austenite (γ) transformation in Fe–C alloys under an external magnetic field

Yinping Zeng[a], Tobias Mittnacht[b], Walter Werner[b], Yong Du[a,*], Daniel Schneider[b,c,*], Britta Nestler[b,c]

[a] State Key Laboratory for Powder Metallurgy, Central South University, Changsha 410083, China
[b] Institute of Applied Materials (IAM-CMS), Karlsruhe Institute of Technology (KIT), Strasse am Forum 7, 76131 Karlsruhe, Germany
[c] Institute of Digital Materials Science (IDM), Karlsruhe University of Applied Sciences, Moltkestr. 30, 76133 Karlsruhe, Germany

Keywords:
thermodynamics
phase-field model
aligned microstructure
magnetic field
Fe–C

Quantitative simulation of microstructure evolution during heat-treatment of alloys under external magnetic field represents a severe challenge. In the present work, the Gibbs free energy contribution from external magnetic field is considered and the experimental Fe–C phase diagram under magnetic field is well reproduced by a thermodynamic model including that contribution. This energy in conjunction with bulk Gibbs energy, demagnetizing field energy and interfacial energy are involved in a developed phase-field model to further bridge the gap between experimental findings and simulative investigations, which is then employed to simulate the microstructure in Fe–C alloys with or without magnetic field. It indicates that the experimental two-phase microstructure (ferromagnetic ferrite α and paramagnetic austenite γ) accompanying the chemically-driven phase transformation in Fe–0.4 and Fe–0.6 wt%C alloys under magnetic field can be quantitatively described by the present phase-field simulation. The predicted phase fraction of ferrite in Fe–C system, which agrees reasonably with the experimental one, is an example to highlight the importance of thermodynamics in tailoring microstructure and properties of realistic alloys with applied magnetic field. This work demonstrates that CALPHAD coupled phase-field model can describe microstructural evolution quantitatively and provides an effective approach for the simulation of corresponding phase transition with external field.

1. Introduction

With the development of superconducting magnets, strong magnetic fields have become easier to achieve and are being utilized in various fields of materials science and engineering. Consequently, a lot of new phenomena have been found by using external magnetic fields during heat-treatment of a variety of materials, and many investigations [1–7] have demonstrated that the applications of external magnetic field can obtain microstructures which are unattainable without magnetic field and thus enhance properties and performance of the materials. Wu et al. [1] reviewed on the magnetic-field-assisted arc welding process and concluded that the external magnetic field could produce positive impacts on arc shape, arc stability and the droplet transfer, improving the microstructure and properties of the arc-welded joint. Recently, a new welding approach with magnetic-field-assisted laser was applied to investigate the weldability of medium-Mn nanostructured steel by Chen et al. [2], who demonstrated that external magnetic field significantly enhances the ultimate strength by 43.9% and dramatically turns the brittle fracture into ductile with a more than tripled elongation rate during uniaxial tension tests. Li et al. [3] reported that preferential (0 0 1) orientation and perpendicular anisotropy can be obtained in $L1_0$ FePt films by using magnetic field annealing, which could be one of promising methods to improve the perpendicular anisotropy for the applications of ultrahigh density magnetic recording media. As a tool to control solidification process, magnetic field can manipulate macroscopic segregation and orientation phenomena [4,5] through magneto-thermodynamics effect, which could effectively avoid defects and inclusions within material [6]. Recently, Hou et al. [7] investigated the influence of axial magnetic field on the structure of directionally solidified Ni–Mn–Ga alloys experimentally. A unique composite structure, which consists of columnar and equiaxed grains, was obtained by them using magnetic-field-assisted directional so-

* Corresponding authors.
E-mail addresses: yong-du@csu.edu.cn (Y. Du), daniel.schneider@kit.edu (D. Schneider).

lidification [7]. It should be mentioned that it is extremely difficult to obtain such a unique composite structure without external magnetic field. This obtained structure enhances mechanical performance, which indicates that the combination of magnetic-field-assisted solidification and subsequent compressive loading can produce dedicated microstructure for the sake of optimizing material properties.

Different kinds of magnetic fields have been utilized in experimental investigations of microstructure and properties optimization [8–13] in several materials. For example, applying a static magnetic field during thermal treatment does alter the microstructure, in particular reduce the width of the long-period stacking ordered laths and thus increase the compression strength of Mg–Al–Gd alloys according to Cai et al. [8]. Traveling magnetic field is considered to be a promising way to control the flows of conductive fluids and the heat/species transport in the melt, and it is thus adapted to explore the microstructure evolution in directionally solidified peritectic Fe–Ni alloys [9]. Under a low growth rate, a rotating magnetic field results in a more uniform eutectic phase distribution and a smaller dendrite arm spacing in solidified Al–7 wt%Si alloy in comparison with the solidification without external magnetic field [10].

To date, researchers mainly focus on experimental aspect of external magnetic fields to search for a desirable combination of alloy composition and heat treatment schedule in order to obtain desired structure for the target materials, while the effect and mechanism of magnetic field on microstructure evolution and mechanical property are poorly understood. Experimentally tailoring the microstructure and properties response of the material under external magnetic fields is costly and extremely time-consuming since many combinations of alloy composition, heat treatment schedule and applied external magnetic field are needed when searching for the best combination. In order to decrease the frequency of trial-and-error experiment as much as possible, most recently, simulations of phase transformations under external magnetic fields have been carried out mainly by means of phase-field approach applied to real materials [14–18]. For example, Koyama and Onodera [14] performed phase-field simulation of twin microstructure evolution in Ni_2MnGa under both stress and magnetic fields. Subsequently, the same group of authors presented phase-field simulations for the modulated structure changes during thermomagnetic treatment and step aging of Fe–Cr–Co alloy [15]. Recently, the modulated microstructure in Alnico alloys reported by Mishima [19] as early as in 1931 was investigated by Sun et al. [16] using both experiment and phase-field method. The total free energy of a system under an applied magnetic field usually includes bulk Gibbs energy of the phase, interfacial energy, elastic energies (in the case of solid state phase transition) and magnetic energy. To the best of our knowledge, in almost all of the previous phase-field simulations, the energy contribution from the magnetic field to the Gibbs energy is not considered since no treatment for such a contribution is available in the literature. This motivates us to focus on the thermodynamic modeling under an external magnetic field and then apply it to phase-field simulation of one target system.

In the present work, the Fe–C alloy is selected as the target system. Extensive experimental investigations [20–25] for this system under magnetic field have been performed on various phase transitions due to its special importance for iron and steel. It is an ideal system to show the effect of magnetic field on microstructure evolution since austenite (γ) is paramagnetic and ferrite (α) is ferromagnetic below Curie temperature. Maruta and Shimotomai [20,21] demonstrated that the aligned γ was obtained by heating via a reverse-transition from lath martensite to ($\alpha+\gamma$) two-phase region in Fe–0.1 wt%C and Fe–0.6 wt%C alloys under the application of a magnetic field. Afterwards, Ohtsuka et al. [22] also confirmed that alignment along the direction of applied magnetic field for Fe–0.4 wt%C alloy is associated with the reverse-transformation. Since no realistic phase-field simulation for microstructure evolution under external magnetic fields has been performed so far, in the present work, a phase-field model linked to CALPHAD (CALculation of PHAse Diagrams)-type thermodynamic parameters considering the effect of magnetic field on Gibbs energy was developed to simulate the morphological evolution during phase transformation of ferrite→austenite in Fe–C alloys. Section 2 details the establishment of a phase-field model under an external magnetic field. In particular, an expression to account for the energy contribution of an external magnetic field to Gibbs energy is described in detail. In Section 3, the phase-field simulations for isothermal growth of austenite particle and morphological evolution in Fe–C alloys with and without external magnetic field are conducted by means of the developed phase-field model. These simulations are compared with corresponding experimental findings. In addition, the role of thermodynamics under external magnetic field for the sake of tailoring microstructure and property is discussed. Section 4 presents the conclusions from the present work.

The main innovation of our work is to model the Gibbs energy contribution from magnetic field and employ this realistic energy to the phase-field simulation for a real system. To the best of our knowledge, such a kind of work is not reported in the literature. The present work not only provides an in-depth understanding of the microstructure evolution in Fe–C system under an external magnetic field, but also establishes a theoretic approach for designing desirable microstructure under external magnetic field through quantitative phase-field simulations.

2. Phase-field model under external magnetic field

2.1. Derivation of the phase-field model

Phase transformation is generally driven by minimization of the total free energy, which consists of bulk Gibbs energy (also named as chemical free energy), interfacial energy and external field energy (such as magnetic energy under an external magnetic field) and so on. In the present work, a new phase-field model, which couples phase-field equations to realistic thermodynamic data under magnetic fields is established, in which the bulk chemical energy, magnetic energy and interfacial energy are considered. Since the use of three energy terms (bulk chemical energy, magnetic energy and interfacial energy) can account for the experimentally observed microstructure [20,22] under external magnetic field, as will be described later, we did not include the elastic contribution to the free energy functional in the phase-field model. It is true that elastic energy does influence the shape of phases involved in solid phase transformation. Our simulation, however, demonstrated that a special shape of the austenite and ferrite phases under the external magnetic field is mainly driven by the magnetic energy. The effect of magnetic field on the shape of austenite and ferrite phases is the main focus of the experimental measurement. Comparing the measured microstructure with/without magnetic field, our phase field simulation results indicate that this kind of directional alignment is formed mainly via external magnetic field. Thus, the elastic contribution to the free energy functional is ignored in the present phase-field simulation.

Two-phase system composed of ferromagnetic ferrite (α) and paramagnetic austenite (γ) phases is considered in the model development. The phase-field and concentration field variables are introduced in the present model. Fig. 1 schematically shows the individual free energy terms and the formation of magnetically aligned microstructure in Fe–C alloys. According to Garcke et al. [26], the total free energy density F_{sys} over the domain Ω for the

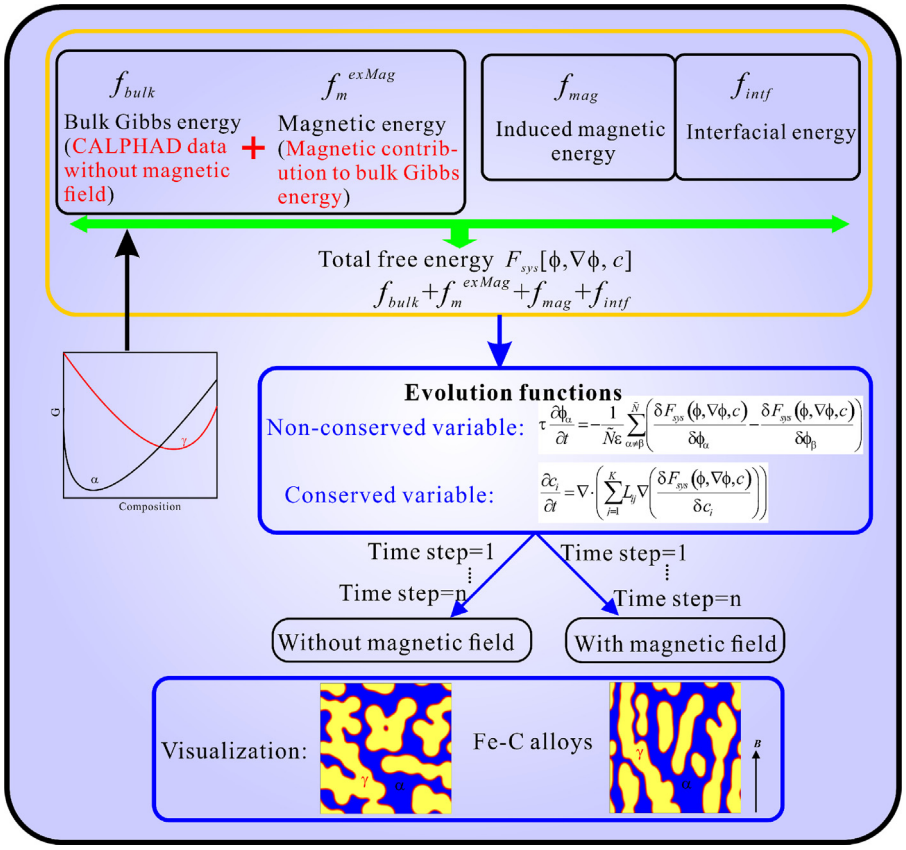

Fig. 1. Flow chart for the phase-field simulation of the aligned microstructure in Fe–C alloys with and without external magnetic field.

target Fe–C system under an external magnetic field can be described as follows:

$$F_{sys}=\int_\Omega\left(f_{intf}+f(\phi,c)+f_{mag}\right)d\Omega \\ =\int_\Omega\left(\varepsilon\alpha(\phi,\nabla\phi)+\frac{1}{\varepsilon}\omega(\phi)+f(\phi,c)+f_{mag}\right)d\Omega \quad (1)$$

where the energy-density contributions from the interfaces and bulk phases are denoted as f_{intf} and $f(\phi, c)$, respectively. ϕ is a phase-field variable which presents phase fraction in the present work, and c is the concentration of carbon. f_{mag} represents the magnetic energy-density induced from the external magnetic field.

It can be seen that the interface contribution comprises of a gradient energy term $\alpha(\phi, \nabla\phi)$ and penalising potential $\omega(\phi)$ in Eq. (1). The gradient energy is expressed with Eq. (2):

$$\varepsilon\alpha(\phi,\nabla\phi)=\varepsilon\sum_{\alpha<\beta}\frac{\gamma_{\alpha\beta}}{m_{\alpha\beta}}a_{\alpha\beta}^2\left|\phi_\alpha\nabla\phi_\beta-\phi_\beta\nabla\phi_\alpha\right|^2 \quad (2)$$

where ε is a length scale parameter related to the thickness of the diffuse interface. $\gamma_{\alpha\beta}$ and $m_{\alpha\beta}$ are dimensionless interfacial energy densities and mobility coefficient, respectively. $a_{\alpha\beta}^2$ depends on the orientation of the interface, and $a_{\alpha\beta}^2=1$ means the isotropic phase boundary applied in the present work.

The potential $\omega(\phi)$ ensures that the value of phase-field is constant at each end of the diffuse interface. In our cases, an obstacle-type potential, as described in Eq. (3), is employed due to its numerical efficiency [27]:

$$\frac{1}{\varepsilon}\omega(\phi)=\frac{16}{\varepsilon\pi^2}\sum_{\alpha<\beta}m_{\alpha\beta}\gamma_{\alpha\beta}\phi_\alpha\phi_\beta+\frac{1}{\varepsilon}\sum_{\alpha<\beta<\delta}\gamma_{\alpha\beta\delta}\phi_\alpha\phi_\beta\phi_\delta \quad (3)$$

where $\gamma_{\alpha\beta\delta}$ means the higher term of interfacial entropy densities to suppress third phase in two-phase interface and usually approximately takes 10 times of $\gamma_{\alpha\beta}$.

The energy contribution of the bulk phases $f(\phi, c)$ in Eq. (1), which is interpolated with phase field parameter ϕ_i, is constructed as a mixture of Gibbs energies for α and γ phases. And it is expressed in Subsection 2.1.2. The Subsection 2.1.1 will detail the description of the magnetic energy f_{mag} induced by the external magnetic field.

The temporal evolution equation [28] for non-conserved phase-field variable is derived by the variational approach and written as:

$$\tau\frac{\partial\phi_\alpha}{\partial t}=-\frac{1}{\tilde{N}\varepsilon}\left(\frac{\delta f_{sys}}{\delta\phi_\alpha}-\frac{\delta f_{sys}}{\delta\phi_\gamma}\right) \quad (4)$$

in which $\tilde{N}$ is the total number of locally active phases and it is 2 within the interfacial regions for the two-phase system in the present simulation, and τ an anisotropic kinetic coefficient with $\tau=\tau(\phi, \nabla\phi)$. For the isotropic case, it becomes $\tau=\tau(\phi)=\frac{\sum_{\alpha<\gamma}\phi_\alpha\phi_\gamma\tau_{\alpha\gamma}}{\sum_{\alpha<\gamma}\phi_\alpha\phi_\gamma}$ with the reciprocal mobility $\tau_{\alpha\gamma}$ of the interface between the phases α and γ.

The evolution equation of the conserved concentration field variable is given by means of Cahn-Hilliard [29] equation:

$$\frac{\partial c_i}{\partial t}=\nabla\cdot\left(\sum_{j=1}^{K}L_{ij}\nabla\left(\frac{\delta f_{sys}}{\delta c_i}\right)\right) \quad (5)$$

i =1,...,K means different components. The superscript K stands for the number of components, and the concentration of components should fulfill the constraint $\sum_{i=1}^{K}c_i=1$ during the evolution. L_{ij} (i, j=1,...,K) is the mobility coefficient and defined as $L_{ij}=\frac{V_m}{R}D(\phi)c_i(\delta_{ij}-c_j)$. The diffusion coefficient is formulated as a linear interpolation across the phases: $D(\phi)=\sum_{\beta=1}^{N}D_{i,\beta}\phi_\beta$, where $D_{i,\beta}$ is the diffusivity of component i in the β phase. For the Fe–C system, component number K is taken as 2 with car-

bon (i=1) and iron (i=2), and diffusion coefficient is given by $D(\phi) = D_{i,\alpha}\phi_\alpha + D_{i,\gamma}\phi_\gamma$ for component i in the two-phase (α+γ) system.

2.1.1. Magnetic energy

The total magnetic energy for a ferromagnetic bulk phase under an external magnetic field includes four parts: external magnetic field energy (also named as Zeeman energy), magnetic exchange energy, magnetic anisotropic energy and demagnetizing field energy. The expressions for these four energy terms are given elsewhere [16]. For the paramagnetic austenite, the total magnetic energy is set to zero due to its weak magnetization at high temperatures. For the ferromagnetic ferrite, external magnetic field energy is involved in the Gibbs energy, which will be described in next subsection. The magnetic anisotropic and magnetic exchange energy are omitted in the present simulation since they do not play important role for the aligned microstructure. Magnetic anisotropy is the energy required to deflect the magnetic moment from the easy magnetization direction to hard magnetization direction. The easy and hard magnetization axes of ferrite are not distinguished and thus are not considered. Under such a treatment, magnetic anisotropic energy is zero. While for the materials which display noticeable magnetic-crystalline anisotropy, magnetic anisotropic energy mainly affects the variant rearrangement for phase. In the late case, this energy term cannot be ignored. The short-range dipole interactions of magnetic moment are described by magnetic exchange energy, which is determined solely by the spatial variation of the magnetization orientation. For the present case, the magnetic moments are perfectly aligned in the same direction of the external magnetic field. This means that this exchange energy could be ignored. As will be described in Subsection 2.1.2, the external magnetic field energy can be added to bulk Gibbs energy. Consequently, except for external magnetic field energy, only demagnetizing field energy is considered in the present work, since it has been understood that the phase transformation associated with the generation and annihilation of the magnetic pole is mainly accounted by the demagnetizing field energy [30]. This kind of field originates from the magnetization, and its direction is opposite to that of the magnetization. When a finite size sample is magnetized by an external magnetic field, a magnetic flux appears inside the sample. It will produce an additional magnetic energy contribution, which is named as demagnetizing field energy. This energy term is represented by an equation of the form:

$$f_{mag} = -\frac{1}{2}\mu_0 H_d M(\phi) \tag{6}$$

where μ_0 and H_d are the vacuum permeability and demagnetizing field strength, respectively. $M(\phi)$ is a magnetization, which depends on temperature and phase-field parameter. For the isothermal simulation, $M(\phi)$ only varies with phase-field values at a fixed temperature. According to magnetic charge method [31], the demagnetizing field strength can be expressed in terms of scalar magnetism potential ψ:

$$H_d = -\nabla\psi \tag{7}$$

and the scalar potential satisfies Poisson's equation:

$$\nabla^2\psi = -\rho \tag{8}$$

wherein $\rho = -\nabla \cdot M(\phi)$ is the magnetic charge density. The driving force ($\frac{\delta f_{mag}}{\delta\phi_\alpha}$) from the demagnetization field can be calculated through Eq. (9), which is derived from Eq. (4). It should be noted that only ferromagnetic α phase contributes to the magnetization for the Fe–C system.

$$\begin{aligned}\frac{\delta f_{mag}}{\delta\phi_\alpha} &= -\frac{1}{2}\mu_0\left(H_d\frac{\partial M(\phi)}{\partial\phi_\alpha} + M(\phi)\frac{\partial H_d}{\partial\phi_\alpha}\right)\\ &= -\frac{1}{2}\mu_0\left[-\nabla\psi\cdot\frac{\partial M(\phi)}{\partial\phi_\alpha} + M(\phi)\frac{\partial(-\nabla\psi)}{\partial\phi_\alpha}\right]\\ &= \frac{1}{2}\mu_0\left[\nabla\psi\cdot\frac{\partial M(\phi)}{\partial\phi_\alpha} + M(\phi)\frac{\partial\nabla\psi}{\partial\phi_\alpha}\right]\end{aligned} \tag{9}$$

Assumptions are made that the saturation magnetization M_s and the Curie temperature T_C in the two-phase region are linear with the content of α phase ϕ_α, and are represented as $M_s = M_\alpha\phi_\alpha$ and $T_C = T_C^\alpha\phi_\alpha$, respectively. Besides, the effect of carbon content on magnetization and Curie temperature for α phase is neglected due to the small solubility of carbon in α phase. Therefore, the magnetization is given by the following equation:

$$M(\phi, T) = M_s m(\Gamma) \tag{10}$$

where $m(\Gamma)$ is the reduced magnetization and obtained as an analytical form, as shown with Eq. (11), on the basis of Weiss molecular field theory [32] which well describes the magnetization of ferromagnetism. Γ is a dimensionless temperature normalized by T_C as $\Gamma = \frac{T}{T_C}$ and approximately described as the following format according to Barsan and Kuncser [33].

$$\begin{aligned}m(\Gamma) &= \left(1 - 2\exp\left(-\frac{2}{\Gamma}\right)\right)\sqrt{1-\Gamma}\\ &\quad\times\left(1 + 0.60683\Gamma - 0.090480\Gamma^2 + 5.9531\Gamma^3\right.\\ &\quad\left.- 11.705\Gamma^4 + 13.950\Gamma^5 - 8.8174\Gamma^6 + 2.2928\Gamma^7\right)(\Gamma \le 1)\\ &= 0 \qquad\qquad (\Gamma > 1)\end{aligned} \tag{11}$$

The parameters $\frac{\partial M}{\partial\phi_\alpha}$, $\nabla\psi$ and $\frac{\partial\nabla\psi}{\partial\phi_\alpha}$ should be provided in order to calculate the magnetic driving force. $\frac{\partial M}{\partial\phi_\alpha}$ could be easily computed and expressed in Eq. (12). As for $\nabla\psi$ and $\frac{\partial\nabla\psi}{\partial\phi_\alpha}$, it is necessary to solve Poisson equation to get the scalar magnetic potential under the assumption that the direction of magnetization is the same as that of the external magnetic field.

$$\begin{aligned}\frac{\partial M}{\partial\phi_\alpha} &= M_\alpha\left(m - \frac{\partial m}{\partial\Gamma}\right)\Gamma \quad (\Gamma \le 1)\\ &= 0 \qquad\qquad\qquad (\Gamma > 1)\end{aligned} \tag{12}$$

2.1.2. Gibbs energy under an external magnetic field

As mentioned before, one innovation of the present phase-field model is to consider Gibbs energy contribution from the external magnetic field for the first time. Such a treatment is not reported in the literature. The Gibbs energy $f(\phi, c)$ of the target system is interpolated with phase-field variables and constructed as a mixture of Gibbs energies for α and γ phases expressed in Eq. (13).

$$\begin{aligned}f(\phi, c) &= \phi_\alpha f_\alpha + \phi_\gamma f_\gamma\\ &= \phi_\alpha\left({}^{0T}f_\alpha + {}^{B}f_\alpha\right) + \phi_\gamma\,{}^{0T}f_\gamma\end{aligned} \tag{13}$$

The Gibbs energies of α and γ include two parts: the Gibbs energy without external magnetic field (${}^{0T}f_i$) and that due to external magnetic field (${}^{B}f_i$). ${}^{0T}f_i$ can be obtained from a thermodynamic description of the Fe–C system [34]. It is worth mentioning that the magnetic field was considered to only affect the Gibbs free energy of α phase since this phase is in ferromagnetic state and the magnetic effect on α phase is more significant than that on paramagnetic γ phase. The contribution of the magnetic field to Gibbs energy for α phase is described by means of Eq. (14):

$${}^{B}f_\alpha = -\int_0^{Bext}\boldsymbol{M}(T, \boldsymbol{B})\mathbf{d}\boldsymbol{B} \tag{14}$$

where $\boldsymbol{B}$ is magnetic flux density and $\boldsymbol{M}$ the magnetization. $\boldsymbol{M}$ depends on temperature and magnetic field $\boldsymbol{B}$, and it is calculated

according to Weiss molecular field theory [32].

$$\boldsymbol{M} = N_A \boldsymbol{m}\left[\frac{2J+1}{2J}coth\left(\frac{2J+1}{2J}\right)\alpha_J - \frac{1}{2J}coth\frac{\alpha_J}{2J}\right]/V_m \tag{15}$$

$$\alpha_J = \frac{\boldsymbol{m}(\boldsymbol{B}+\lambda\boldsymbol{M})}{k_B T} \tag{16}$$

$$\lambda = \frac{3V_m J k_B T_C}{N_A \boldsymbol{m}^2 (J+1)} \tag{17}$$

wherein N_A represents Avogadro constant and $\boldsymbol{m}$ denotes atomic magnetic moment. J is the quantum number related to the angular momentum of an atom. λ is the molecular field constant, V_m denotes the molar volume, T_C Curie temperature and k_B the Boltzmann constant. Numerical fitting was employed for the calculation of magnetic free energy owing to the difficulty of solving complex implicit Brillouin functions.

For almost all of the phase-field simulations under an external magnetic field reported in the literature, the Gibbs energy in the phase-field model only involves the Gibbs energy without external magnetic field (^{0T}f). Such a treatment is not physically sound. In the present work, we have proposed a method to describe the contribution of the external magnetic field to the bulk Gibbs energy.

2.2. Procedure for the phase-field simulation

The "Parallel Algorithms for Crystal Evolution in 3D" (PACE3D) framework, which provides a combined solution with a wide range of easy to use extensible models to solve multi-physics application in a parallel and efficient manner [35], is utilized in the present simulation. Solver [36–40] structure in PACE3D contains diffuse interface approaches, grain growth, grain coarsening, solidification, fluid flow, mechanical forces, and electrochemistry and so on. The framework allows the implementation of new phase-field models for describing different processes. In the present work, the calculation of driving force from the demagnetizing field is implemented for the related simulation, as shown in the chart flow illustrated in Fig. 1.

A two-dimensional simulation box with 100 × 100 cells along the x and y directions is firstly considered to study the effect of magnetic field on the microstructure of solid phase transformation. The little circular inclusion of the productive particle will grow in the parent ferrite α matrix under the integrated driving force from chemical energy, interfacial energy and magnetic field energy if magnetic field is turned on. After that, the CALPHAD type data for the Fe–C system with or without magnetic field was applied in order to describe the microstructure evolution quantitatively. For numerical efficiency, the Gibbs free energy data are parabolically approximated and then the fitted Gibbs free energy was applied to the further simulation of the two-phase microstructure in the absence of or with magnetic field in a 2D domain of dimensions 300 × 300. The initial structure is generated using a voronoi tessellation based on a random set of points. It is noteworthy that periodic boundary conditions were applied along both x and y directions. Table 1 summarizes the model parameters employed in the present simulation. Temperature and alloy composition are chosen according to experimental information. Curie temperature and magnetic moment for α phase are taken as the corresponding values of pure Fe in view of the very small solubility of C in α phase. Grid cell size Δx takes 5, and time step width Δt is set as $0.1(\Delta x)^2$. Length scale parameters ε is $3.5\Delta x$. Anisotropic kinetic coefficient τ and interfacial energy density $\gamma_{\alpha\beta}$ depend on temperature for simulation at different temperatures and are taken as $1.066 \times 10^{-3}T$ and $3.2 \times 10^{-6}T$, respectively.

Table 1
Numerical parameters used in the present phase-field simulation

Parameters (Unit)	Symbol	Value	
Temperature (K)	T	1023	1018
Composition		0.4 wt%C	0.6 wt%C
Magnetic field (Tesla T)	$\boldsymbol{B}$	10	8
Simulation domain		300 × 300	
Curie temperature for α phase (K)	T_C^{α}	1043	
Magnetic moment for α phase	M_α	2.22	
Anisotropic kinetic coefficient	τ	$1.066 \times 10^{-3}T$	
Length scale parameter (m)	ε	1.75×10^{-5}	
Time step width	Δt	2.5	
Grid cell size (m)	Δx	5×10^{-6}	
Interfacial energy density (J/m^2)	$\gamma_{\alpha\beta}$	$3.2 \times 10^{-6}T$	

3. Results and discussion

3.1. Simulation of isothermal growth of an austenite particle

To successfully reproduce the aligned microstructure evolution with the effect of magnetic field by means of the presently developed phase-field model, we first simulated the isothermal growth of a circle austenite particle in 100 × 100 domain at 1023 K. This kind of preliminary calculation could provide reasonable parameters for the more complex simulation with a larger domain. The first row displayed in Fig. 2 is the $\alpha \rightarrow \gamma$ phase transformation without magnetic field, and second row shows the corresponding microstructure evolution under the influence of magnetic field. For both simulations, the input parameters, apart from those associated with magnetic field, are similar to ensure comparability. Hereafter, the time unit in this figure denotes dimensionless time. It can be obviously seen that the austenite γ phase expands with an isotropic pattern in the absence of magnetic influence, while it grows ellipsoidally-shaped and finally aligns perfectly in the direction of magnetic field. It indicates that the simulated directionally aligned two-phase microstructure owing to magnetic field agrees with the experimental observation.

As shown in Figs. 3(a) and (b), which characterize the growth of austenite in horizontal and vertical directions corresponding to y=50 and x=50 (The black lines in Fig. 2) without magnetic field, respectively, we can see that diffuse interface moves simultaneously in both x and y axis with the same rate in the absence of magnetic field. The same rate in both x and y directions means that austenite particle grows isotropically. In the case of the calculations under the impact of magnetic field, as shown in Figs. 3(c) and (d), it is indicated that austenite particle grows much slower perpendicular to the magnetic field direction than the one in the direction of magnetic field. A possible explanation for this phenomenon could be that additional demagnetizing field energy of ferrite in the direction of magnetic field destabilizes ferrite more than that in perpendicular direction, which accelerates the phase transition parallel to the magnetic field. Figs. 2-3 indicate that the application of magnetic fields during the $\alpha \rightarrow \gamma$ isothermal transformation in Fe–C alloys develops a two-phase microstructure with the paramagnetic γ phase aligned in the matrix of the ferromagnetic α phase along the direction of applied magnetic field. Consequently, it is expected that the experimentally observed aligned microstructure could be accounted for by means of phase-field approach using the three energy terms of bulk chemical, magnetic and interfacial energies.

3.2. Morphological evolution in Fe–C alloys with and without external magnetic field

In order to increase the numerical efficiency for large-scale phase-field simulations, the thermodynamic parameters which de-

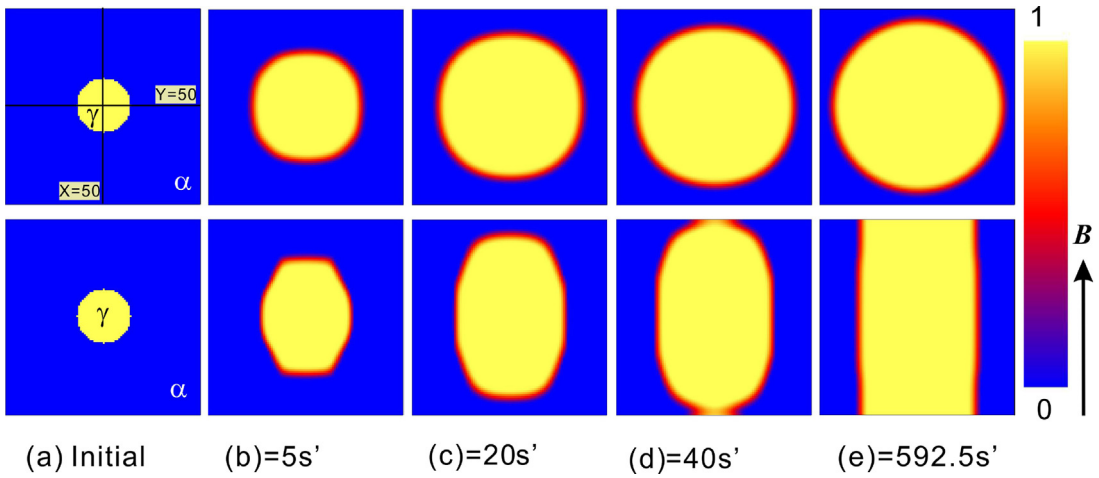

Fig. 2. The growth of an austenite γ particle inside the ferromagnetic ferrite α against time with/without magnetic field. The first row shows the calculations without magnetic field and the second with the magnetic field applied to the direction parallel to y axis.

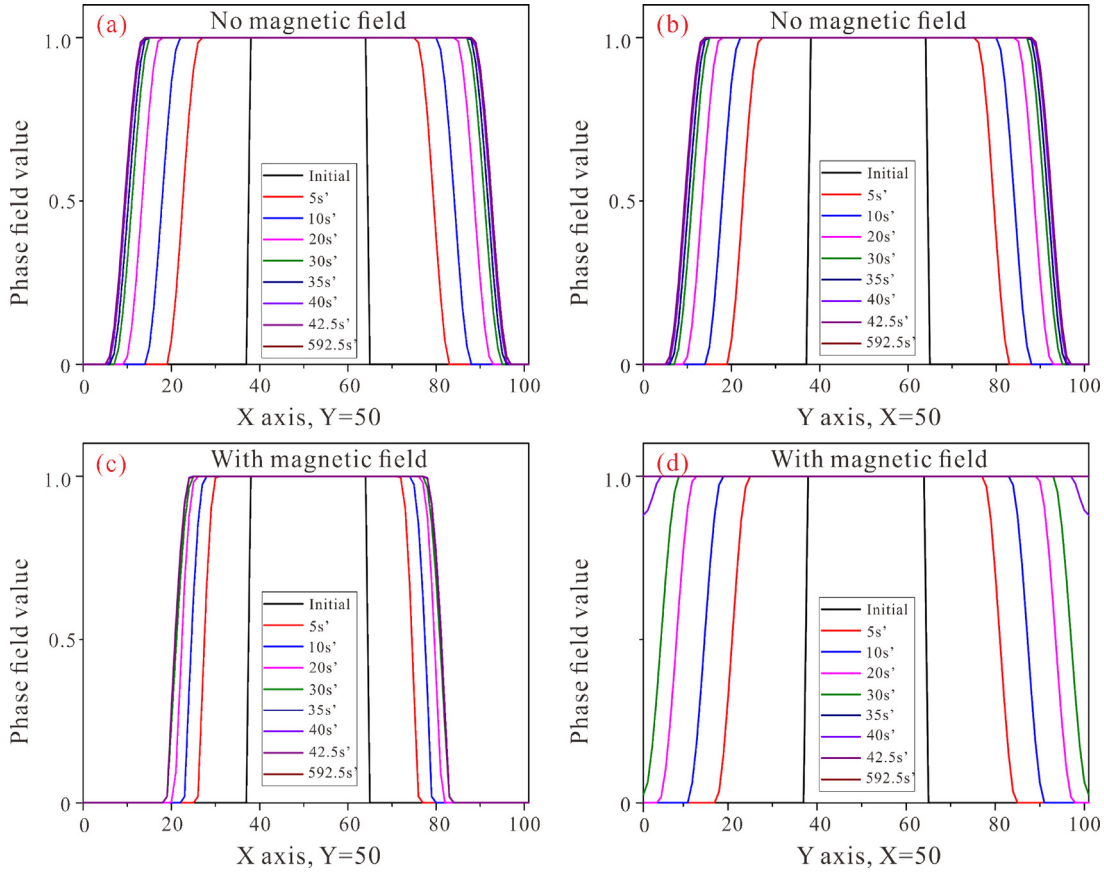

Fig. 3. The grow rate of austenite particle along X=50 and Y=50. Without magnetic field (a) X axis, Y=50 and (b) Y axis, X=50; with magnetic field (c) X axis, Y=50 (perpendicular to the magnetic field) and (d) Y axis, X=50 (along the direction of magnetic field).

scribe the Gibbs energies of α and γ phases were not used directly in the simulations, but parabolic format of the energy for target phases is employed [34].

Fig. 4 displays the Gibbs energy of α phase under the magnetic field of 10 T (Tesla) including Eq. (13) together with the energy of γ phase at 1023 and 1018 K. The calculations indicate that magnetic field decreases the energy of α phase and the tendency increases with increasing magnetic field. Many experiments [41–43] have confirmed that a magnetic field reduces the free energy of α phase in steels, being consistent with the present calculations. The concentrations of carbon in α and γ will increase with applied magnetic field according to common tangent principle. It has been clarified that the driving force of a transformation depends on the Gibbs free energy difference between the product and the parent phases. The application of magnetic field increases the total Gibbs free energy difference between α and γ which means that the equilibrium temperature lines between α and γ in the phase diagram moves to high temperature side. And the solubility of C in both α and γ would increase, even though the sharp boundary line between α and $\alpha+\gamma$ phase regions causes the unobvious increased

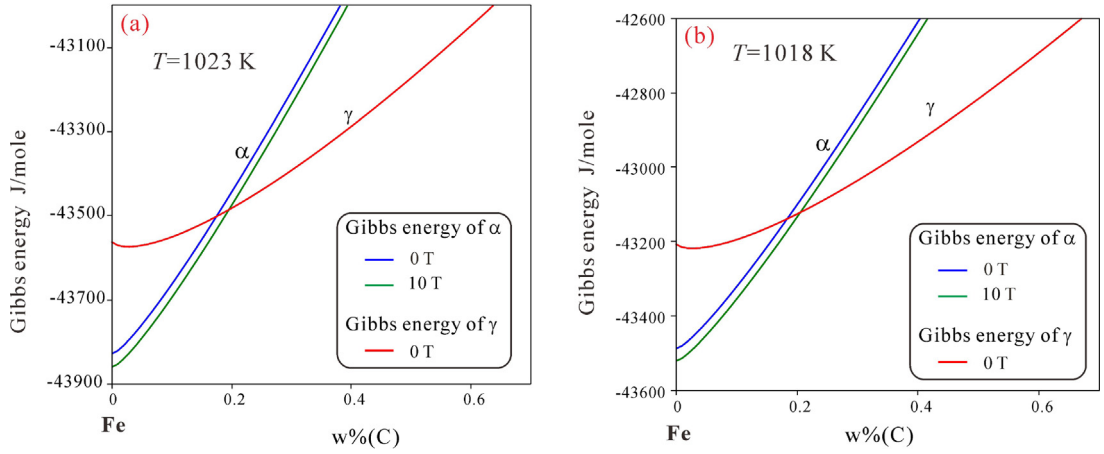

Fig. 4. Gibbs energy curve of α phase under 0 and 10 T magnetic field along with the Gibbs energy of γ phase: (a) 1023 K and (b) 1018 K.

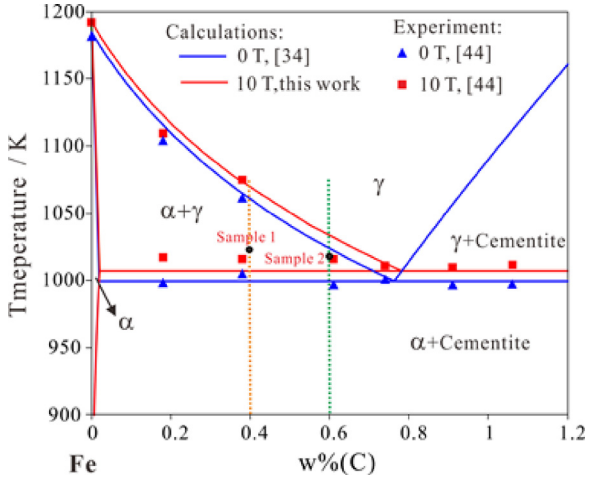

Fig. 5. Calculated Fe–C phase diagram under external magnetic field. The blue lines without the magnetic field are according to the calculations using the parameters from Gustafson [34], and red lines are according to the present work considering the external magnetic field. Blue triangle and red square stand for the experimental data [44], and black dots indicate the location of the samples.

C solubility of α from the phase diagram. On the other hand, the magnetic contribution to Gibbs free energy for both γ and cementite is ignored. As a result, the driving force for transformation from γ to cementite is not affected by the applied magnetic field. Hence the equilibrium line between cementite and γ remained unchanged. Consequently, the phase equilibrium of the Fe–C system under a magnetic field will be different from that without magnetic field. Fig. 5 demonstrates the calculated Fe–C phase diagram under 0 and 10 T together with experimental data [44], including the compositions of target alloys also. It can be seen that samples Fe–0.4 wt%C and Fe–0.6 wt%C are located in $(\alpha+\gamma)$ two-phase region. It is indicated that the magnetic field alters volume fractions of the phases according to lever rule and solubility of carbon at two-phase equilibrium, and also shifts the eutectoid composition to higher carbon content.

The Gibbs energy curves in Fig. 4 are approximately expressed in second order polynomial, which is an established method in phase-field model to capture concentration dependent energy characteristics. For the phase-field simulation of microstructure in the Fe–C alloys, the employed model parameters are listed in Table 1. Two-dimensional simulations of microstructure development in Fe–0.4 wt%C at 1023 K and Fe–0.6 wt%C at 1018 K without or with external magnetic field are shown in Figs. 6 and 7, respectively. The sequence of phase transformation and microstructure evolution are represented from (a) to (e). It manifests the temporal evolution of the phase field ϕ_i together with the experimental microstructure [20–22], and the blue and yellow regions denote α and γ phases, respectively. The temporal development of carbon concentration is similar to that in Figs. 6-7, which is displayed in Figs. 8-9 and facilitates the understanding of carbon distribution within the two phases.

The left columns displayed in Figs. 6 and 7 are the morphological evolution in Fe–0.4 wt%C and Fe–0.6 wt%C alloys without magnetic field. At an initial state, supersaturated ferrite α and seeds of austenite γ are given. During aging, supersaturated ferrite transforms into austenite due to the decrease of total energy, and the volume fraction of γ phase increases from (a) to (e). γ phase grows gradually in each direction, which is accompanied by coalescing behavior with increasing aging time. The right rows in Figs. 6 and 7 show the phase-field simulated microstructure development in Fe–0.4 wt%C under 10 T and Fe–0.6 wt%C under 8 T, respectively. The applied magnetic field is in vertical direction. The figures demonstrate that the simulated two-phase microstructure formed under the influence of magnetic field are in reasonable agreement with experimental observation [20–22]. Supersaturated ferrite transformed into austenite and the produced austenite phase grows faster in the direction of magnetic field. This kind of alignment is considered to be induced by the dipolar interactions between matrix and precipitate [20,21,23]. The corresponding evolution of carbon profile is presented in Figs. 8 and 9 for Fe–0.4 wt%C and Fe–0.6 wt%C, respectively. As the diffusion of carbon, which is not directly affected by magnetic field since carbon is nonmagnetic, the demagnetizing field energy expressed by Eq. (6) only depends on local phase fraction ϕ_α since α phase contributes to Curie temperature and magnetization of the two-phase system. And the influence from magnetic field on the diffusion behavior of carbon is reflected through the phase-field variable since the mobility coefficient in governing equation is defined with ϕ_i.

After extended periods of annealing, simulations would reach equilibrium under the cooperation of chemical and magnetism, which influence diffusion, equilibrium compositions and driving force. For Fe–0.4 wt%C alloy, the volume fraction V_f of austenite without magnetic field reaches the equilibrium value faster than that under 10 T. And the increasing rate of volume fraction for the simulation without magnetic field is larger than the one considering the effect of magnetic field, which means that magnetic field influences the rate of phase transformation. Additionally, the volume fraction and carbon concentration in α and γ phases simulated by phase-field method for Fe–0.4 wt%C alloy are quantitatively compared with thermodynamic calculation for the equilib-

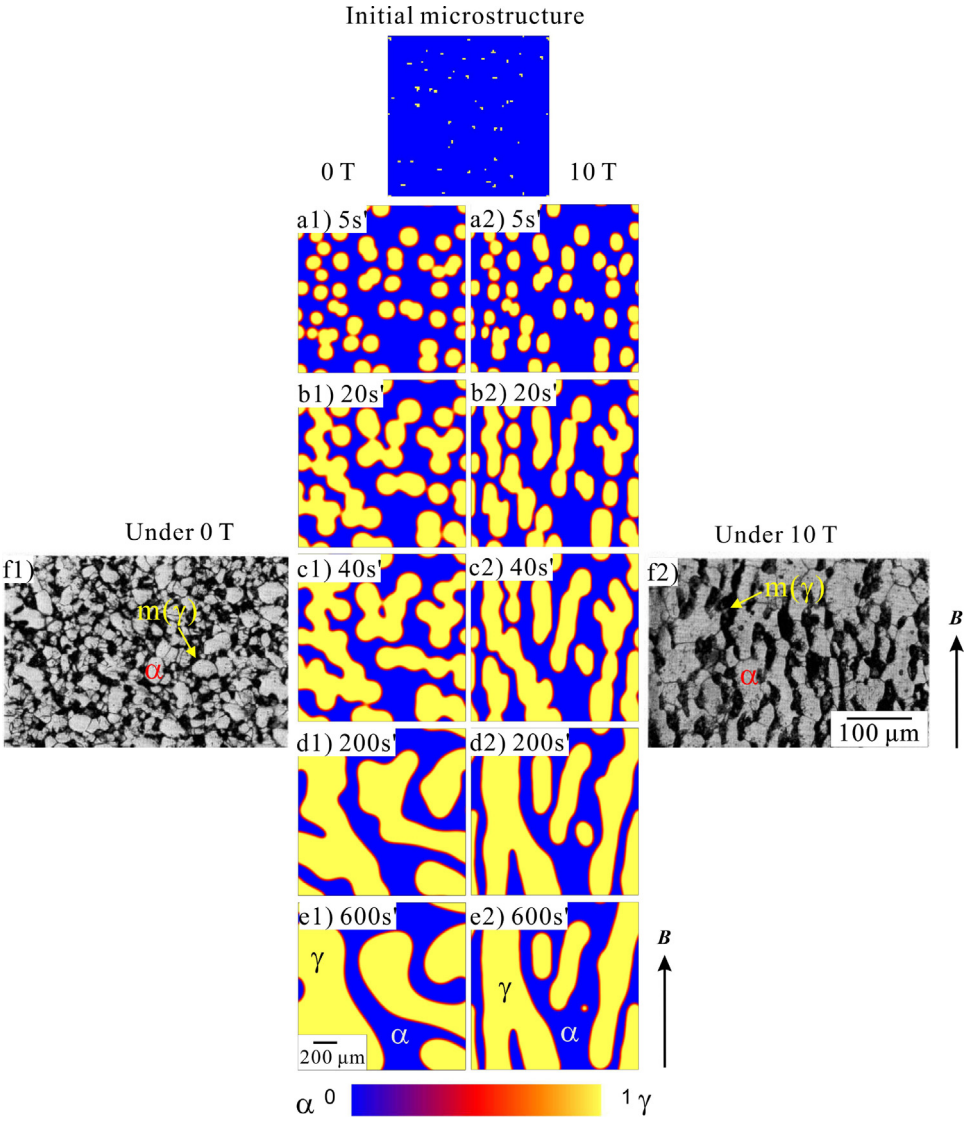

Fig. 6. The evolution of microstructure in Fe–0.4 wt%C aging at 1023 K with 10 T and without the influence of magnetic field. No magnetic field: (a1-e1); magnetic field: (a2-e2). Figs. f1 and f2 are reproduced from Ref. [22].

Table 2
Comparison of $\alpha+\gamma$ two-phase equilibrium between thermodynamic calculation and phase-field simulation*

Sample	Thermodynamic calculation		Phase-field simulation	
	No magnetic field	With magnetic field	No magnetic field	With magnetic field
1023 K	x(α,C)= 0.00078	x(α,C)= 0.00088	x(α,C)= 0.00081	x(α,C)= 0.00082
0.4 wt%C	x(γ,C)= 0.02748	x(γ,C)= 0.03032	x(γ,C)= 0.02780	x(γ,C)= 0.02895
	V(γ)=0.66	V(γ)=0.60	V(γ)=0.59	V(γ)=0.60
	x(C) = 0.01831	x(C)= 0.01831	x(C)= 0.01673	x(C)= 0.0174
1018 K	x(α,C)= 0.00080	x(α,C)= 0.00085	x(α,C)= 0.00078	x(α,C)= 0.00079
0.6 wt%C	x(γ,C)= 0.02890	x(γ,C)= 0.0305	x(γ,C)= 0.02917	x(γ,C)= 0.02936
	V(γ)=0.94	V(γ)=0.89	V(γ)=0.94	V(γ)=0.90
	x(C)= 0.0273	x(C)= 0.0273	x(C)= 0.0273	x(C)= 0.0264

* 10 and 8 T are applied for the thermodynamic calculation of Fe–0.4 wt%C and Fe–0.6 wt%C alloys, respectively. x(α,C) and x(γ,C) mean the mole fraction of carbon in α and γ phases, respectively. x(C) denotes the alloy composition, and V(γ) is the volume fraction of γ phase.

rium state, which is demonstrated in Table 2. As for the simulation of Fe–0.6 wt%C without magnetic field, the V_f of austenite is taken the same value from thermodynamic result, and the corresponding distributions of carbon data are used as the equilibrium data since ferrite would vanish with V_f more than 0.94 for austenite in phase-field simulation. It can be seen that the modeled volume fractions of austenite and ferrite agree well with thermodynamic calculation results, and that of austenite in Fe–0.6 wt%C alloy is larger than that in Fe–0.4 wt%C, which can be easily understood in view of lever rule. The content of carbon in ferrite and austenite increases with the effect of magnetic field due to the chemical effect from the application of magnetic field, which can be comprehended from the phase diagram.

The present work demonstrates that the phase-field model considering the contribution of external magnetic field to Gibbs energy can not only reproduce the phase diagram, but also describe mi-

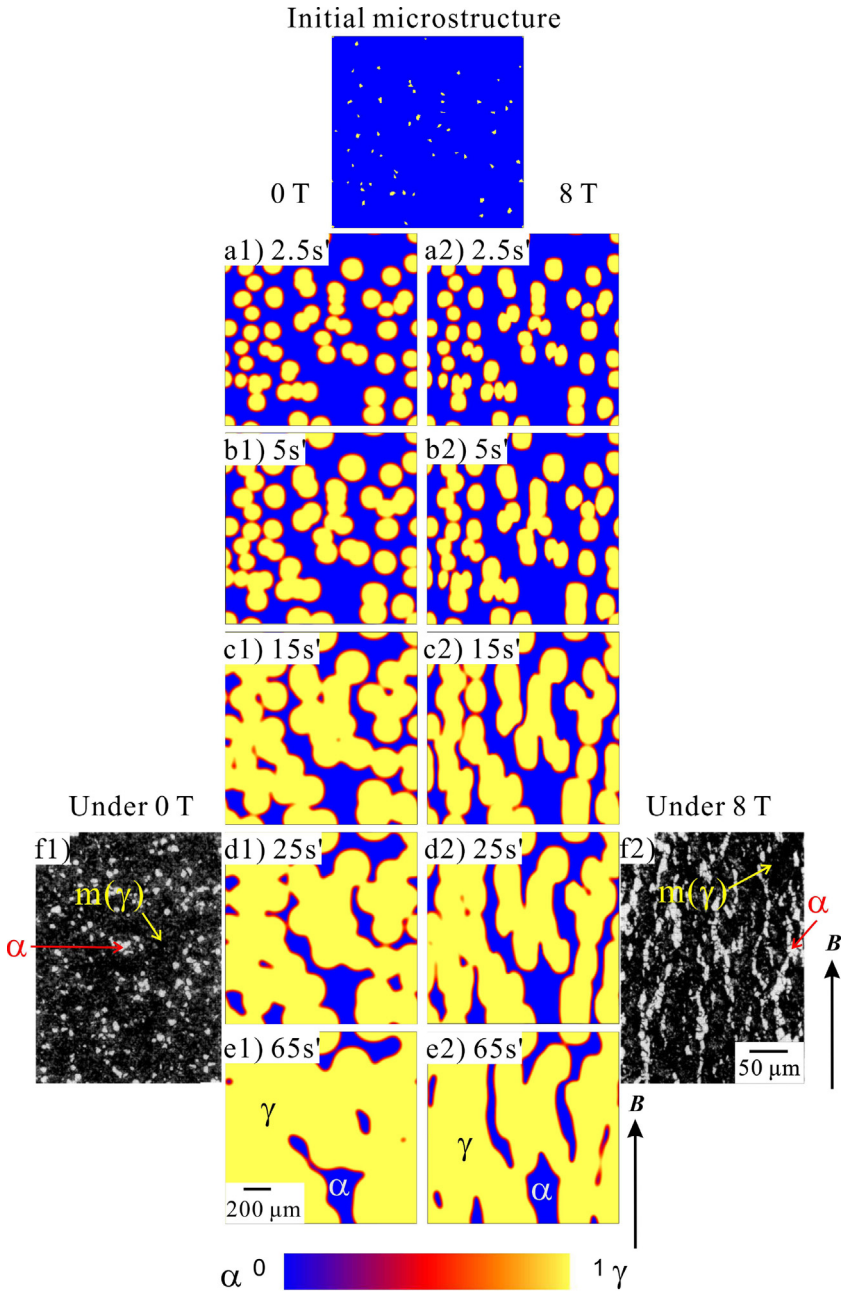

Fig. 7. The evolution of microstructure in Fe–0.6 wt%C aging at 1018 K with 8 T and without the influence of magnetic field. No magnetic field: (a1-e1); magnetic field: (a2-e2). Figs. f1 and f2 are reproduced from Ref. [20].

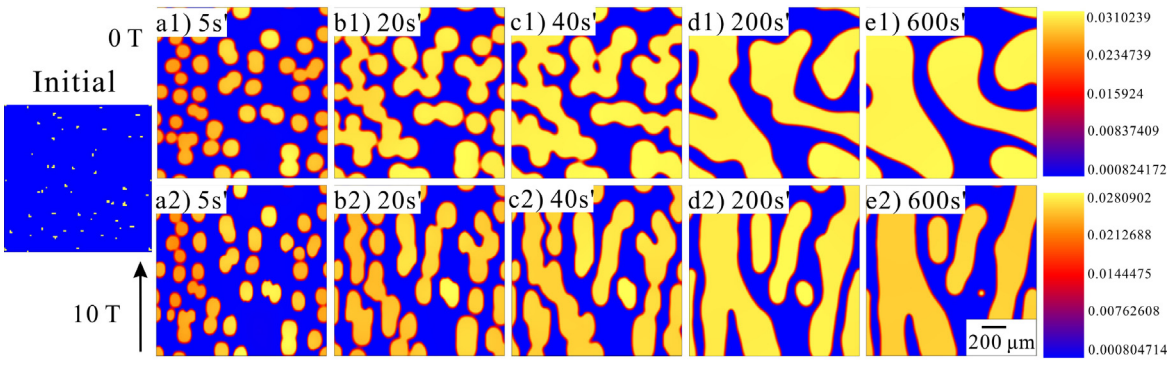

Fig. 8. The evolution of carbon profile in ferrite and austenite in Fe–0.4 wt%C aging at 1023 K with and without the influence of magnetic field. No magnetic field: (a1-e1); magnetic field: (a2-e2).

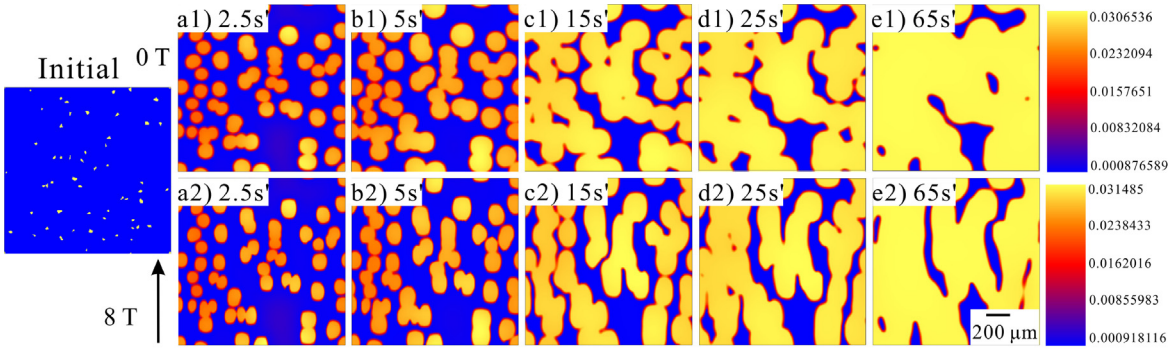

Fig. 9. The evolution of carbon profile in ferrite and austenite in Fe–0.6 wt%C aging at 1018 K with and without the influence of magnetic field. No magnetic field: (a1-e1); magnetic field: (a2-e2).

crostructure in Fe–C alloys quantitatively under the external magnetic field for the first time.

3.3. The role of thermodynamics in tailoring microstructure and property under magnetic field

Thermodynamics under magnetic field is important for the magnetic-field-assisted experimental investigation since phase transformation has a strong influence on the mechanical property of alloys, such as high entropy alloy (HEA) and steel. As for AlCoCrFeNi HEA, mechanical behavior is significantly affected by composition and heat treatment temperature, and the utilization of magnetic field at specific temperature can lead to the energy difference among ferromagnetic Bcc, paramagnetic Fcc and σ phases and thus change the phase fractions of these phases. According to Zhao et al. [45], an excellent combination of saturation magnetization, electrical resistivity, yield strength, ultimate compressive strength and compressive plastic strain was achieved when applying 6 T magnetic field at heat-treatment temperature of 1200 °C for AlCoCrFeNi HEA. Precipitation behavior of transition carbides in steel controls material property. The introduction of magnetic field can effectively change their stability by altering their free energy levels due to their magnetization degrees. These studies [46,47] have revealed that the applied magnetic field effectively promotes the precipitation of χ-Fe_5C_2 iron carbide, compared to the usual ε-Fe_2C and η-Fe_2C iron carbides, because the higher magnetization resulted in the remarkable reduction of free energy for χ-Fe_5C_2 carbide.

The magnetic field increases the carbon solubility in ferrite which has been discussed in Subsection 3.2 and thus enhances the hardness for ferrite. The hardness values of ferrite formed under 10 T showed consistently higher values compared to that without magnetic field according to the work from Choi et al. [48]. As demonstrated in Fig. 5, a magnetic field would shift the eutectoid composition to higher carbon content, which indicates the increase of carbon content without hypereutectoid transformation, and thus provides the possibility of improving mechanical properties since increased carbon content is associated with strengthening and hardening. On the other hand, hypereutectoid primary cementite decreases ductility. Fig. 10 presents the calculated phase fraction of α in Fe–0.6 wt%C sample against the temperature under magnetic field together with the experimental data [20]. It can be seen that the calculation agrees well with experimental observation except for the calculated result under 8 T. The calculations associated with 8 T also can be accepted since the temperature discrepancy between calculation and experiment for the phase transition $\gamma \rightarrow \gamma + \alpha$ is generally within 5 °C. It is clear that magnetic field increases the phase fraction of ferrite and eutectoid temperature, which indicates that austenite to pearlite transformation occurs at

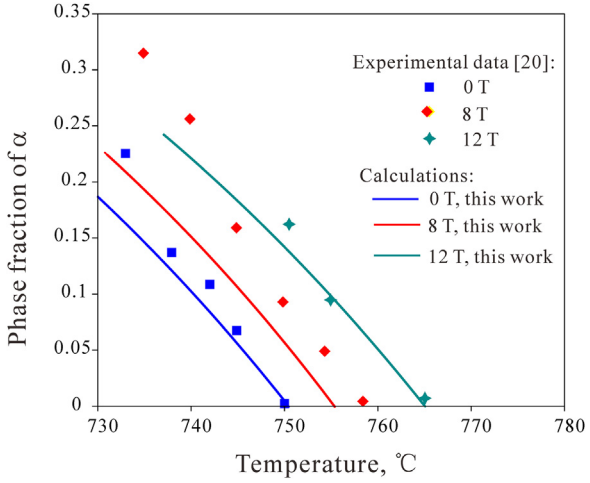

Fig. 10. Calculated phase fraction of ferrite α in Fe–0.6 wt%C alloys versus temperature under magnetic field in comparison with the experimental data [20]. Along the solid lines, there are equilibria between α and γ phases.

higher temperature. The austenite to pearlite transformation is diffusional and involves the cooperative formation of carbon-depleted ferrite and carbon-enriched cementite. The inter-lamellar spacing of the pearlite depends on the diffusion distance of the carbon. The higher formation temperature allows greater carbon diffusion and then increases the inter-lamellar spacing, thus modifies mechanical properties. Fig. 10 demonstrates that thermodynamic calculation for Fe–C alloy under magnetic field can predict the phase fraction for specific magnetic field and alloy composition, which provides the possibility to obtain the desirable combination of heat-treatment schedule and alloy composition with the assessment of magnetic field for the sake of material design.

4. Conclusions

The present work is the first attempt to consider the Gibbs energy contribution from magnetic field and apply it to simulate the microstructure evolution of realistic Fe–C system under external magnetic field by means of phase-field approach. The main conclusions are as follows:

- The Gibbs energy contribution from magnetic field for ferromagnetic α phase is calculated based on Weiss molecular theory. The computed Fe–C phase diagram under magnetic field agrees reasonably with the experimental data. The thermodynamic description under magnetic field is utilized in phase-field model for Fe–C system for the first time.

- The microstructure formed during thermomagnetic treatment for Fe–0.4 wt%C and Fe–0.6 wt%C alloys are quantitatively performed by phase-field method combined with CALPHAD type thermodynamic data, and the simulated microstructure is in reasonable agreement with the experimental investigation. The structural alignment of $(\alpha+\gamma)$ microstructure under the influence of magnetic field indicates that modeling microstructure developments with the frameworks of phase-field approach is a very effective strategy to analyze complex microstructure. In particular, the phase-field simulation coupled with realistic thermodynamic database is quite helpful to design the microstructure in realistic alloys.
- The increased carbon solubility in ferrite and eutectoid temperature under the influence of magnetic field enables researchers to enhance the property of steel. This explains the important role of thermodynamics in tailoring microstructure and property under magnetic field.

Declaration of Competing Interest

The authors declare that they have no known conflict financial interests or personal relationships that could have appeared to influence the work reported in this paper.

Acknowledgements

The authors would like to thank Professor Dr. Rainer Schmid-Fetzer from Clausthal University of Technology in Germany for guiding the thermodynamic calculation involving magnetic field. The financial support from National Key Research and Development Program (Grant No. 2019YFC1904901) and National Natural Science Foundation of China (Grant no. 51820105001) are acknowledged. Yinping Zeng is grateful for the scholarship from China Scholarship Council, which pursues her study at Karlsruhe Institute of Technology in Germany from Oct. 2019 to Oct. 2020.

References

[1] H. Wu, Y. Chang, L. Lu, J. Bai, Review on magnetically controlled arc welding process, Int. J. Adv. Manuf. Technol. (2017).
[2] R. Chen, H.J. Kong, J.H. Luan, A.D. Wang, P. Jiang, C.T. Liu, Effect of external applied magnetic field on microstructures and mechanical properties of laser welding joint of medium-Mn nanostructured steel, Mater. Sc. Eng., A 792 (2020) 139787.
[3] Y.B. Li, Y.F. Lou, L.R. Zhang, B. Ma, J.M. Bai, F.L. Wei, Effect of magnetic field annealing on microstructure and magnetic properties of FePt films, J. Magn. Magn. Mater. 322 (23) (2010) 3789–3791.
[4] S. Dutta, A.K. Panda, S. Chatterjee, R.K. Roy, Effect of annealing treatment on magnetic texture of cold rolled ULC steel, Mater. Lett. 276 (2020) 128211.
[5] C. Wei, J. Wang, Y. He, J. Li, E. Beaugnon, Influence of high magnetic field on the liquid-liquid phase separation behavior of an undercooled Cu–Co immiscible alloy, J. Alloys Compd. (2020) 155502.
[6] X. Yu, Z. Wang, Z. Lu, Atmospheric corrosion behavior of copper under static magnetic field environment, Mater. Lett. 266 (2020) 127472.
[7] L. Hou, Y. Dai, Y. Fautrelle, Z. Li, X. Li, Control of microstructure using magnetic fields and study of the mechanical behavior of Ni-rich Ni-Mn-Ga alloys, Acta Mater 199 (2020).
[8] Q. Cai, C. Zhai, Q. Luo, T. Zhang, Q. Li, Effects of magnetic field on the microstructure and mechanical property of Mg-Al-Gd alloys, Mater. Charact. 154 (2019) 233–240.
[9] Q. Ling, J. Shen, Z. Feng, S. Zhao, H. Fu, Microstructure evolution in directionally solidified Fe–Ni alloys under traveling magnetic field, Mater. Lett. 115 (jan.15) (2014) 155–158.
[10] Y.Z. Li, N. Mangelinck-Noel, G. Zimmermann, L. Sturz, H. Nguyen-Thi, Modification of the microstructure by rotating magnetic field during the solidification of Al-7 wt.% Si alloy under microgravity, J. Alloys Compd. 836 (2020) 155458.
[11] Y. Dong, S. Shuai, J. Yu, W. Xuan, Z. Zhang, J. Wang, Z. Ren, Effect of high static magnetic field on the microstructure and mechanical properties of directional solidified alloy 2024, J. Alloys Compd. 749 (2018) 978–989.
[12] H. Technology, The Influence of Traveling Magnetic Field on Solidification Defects and Mechanical Properties of ZL205A Alloy Sheet Casts, Rare Met. Mater. Eng. 43 (11) (2014) 2602–2608.
[13] J.C. Jie, Q.C. Zou, J.L. Sun, Y.P. Lu, T.M. Wang, T.J. Li, Separation mechanism of the primary Si phase from the hypereutectic Al–Si alloy using a rotating magnetic field during solidification, Acta Mater 72 (2014) 57–66.
[14] T. Koyama, H. Onodera, Phase-Field Simulation of Microstructure Changes in Ni2MnGa Ferromagnetic Alloy Under External Stress and Magnetic Fields, Mater. Trans. 44 (12) (2005) 2503–2508.
[15] T. Koyama, H. Onodera, Modeling of microstructure changes in FeCrCo magnetic alloy using the phase-field method, J. Phase Equilib. Diffus. 27 (1) (2006) 22–29.
[16] X.Y. Sun, C.L. Chen, L. Yang, L.X. Lv, S. Atroshenko, W.Z. Shao, X.D. Sun, L. Zhen, Experimental study on modulated structure in Alnico alloys under high magnetic field and comparison with phase-field simulation, J. Magn. Magn. Mater. 348 (2013) 27–32.
[17] T. Koyama, H. Onodera, Phase-field Modeling of Structural Elongation and Alignment of $(\alpha+\gamma)$ Microstructure in Fe–0.4C Alloy during Thermomagnetic Treatment, ISIJ Int 46 (9) (2006) 1277–1282.
[18] Z. Feng, Y. Hong, G. Wang, X. Wu, D. Zeng, Effects of external magnetic field on the solidification process in Nd–Fe–B alloy: phase-field simulation, Modell. Simul. Mater. Sci. Eng. 26 (2018) 025012.
[19] T. Mishima, Nickel-aluminum steel for permanent magnets, Stahl und Eisen 53 (1931) 79.
[20] K.I. Maruta, M. Shimotomai, Alignment of Two-Phase Structures in Fe–C Alloys by Application of Magnetic Field, Mater. Trans. JIM 41 (8) (2000) 902–906 JIM.
[21] M. Shimotomai, K. Maruta, Aligned two-phase structures in Fe-C alloys, Scripta Mater 42 (5) (2000) 499–503.
[22] H. Ohtsuka, Y. Xu, H. Wada, Alignment of ferrite grains during austenite to ferrite transformation in a high magnetic field, Mater. Trans. JIM 41 (8) (2000) 907–910 JIM.
[23] K. Maruta, M. Shimotomai, Magnetic field-induced alignment of steel microstructures, Journal of Crystal Growth 237 (2002) 1802–1805.
[24] X.J. Hao, H. Ohtsuka, P.D. Rango, H. Wada, Quantitative Characterization of the Structural Alignment in Fe0.4C Alloy Transformed in High Magnetic Field, Mater. Trans. 44 (1) (2003) 211–213.
[25] M. Shimotomai, K. Maruta, K. Mine, M. Matsui, Formation of aligned two-phase microstructures by applying a magnetic field during the austenite to ferrite transformation in steels, Acta Mater 51 (10) (2003) 2921–2932.
[26] H. Garcke, B. Nestler, B. Stoth, A MultiPhase Field Concept: Numerical Simulations of Moving Phase Boundaries and Multiple Junctions, SIAM J. Appl. Math. 60 (1) (1999) 295–315.
[27] A. Choudhury, B. Nestler, Grand-potential formulation for multicomponent phase transformations combined with thin-interface asymptotics of the double-obstacle potential, Phys. Rev. E 85 (2012) 021602.
[28] I. Steinbach, Phase-field models in materials science, Modell. Simul. Mater. Sci. Eng. 17 (7) (2009) 073001.
[29] J.W. Cahn, J.E. Hilliard, Free Energy of a Nonuniform System. I. Interfacial Free Energy, J. Chem. Phys 28 (2) (1958) 258–267.
[30] J.W. Cahn, Magnetic Aging of Spinodal Alloys, J. Appl. Phys. 34 (1963) 3581–3586.
[31] J.M. Coey, Magnetism and magnetic materials, Cambridge university press, 2010.
[32] B.D. Cullity, C.D. Graham, Introduction to magnetic materials, Wiley, Hoboken, 2009.
[33] V. Barsan, V. Kuncser, Exact and approximate analytical solutions of Weiss equation of ferromagnetism and their experimental relevance, Philos. Mag. Lett. 97 (9) (2017) 359–371.
[34] P. Gustafson, Thermodynamic evaluation of the Fe-C system, Scand. J. Metall. 14 (5) (1985) 259–267.
[35] J. HoTzer, A. Reiter, H. Hierl, P. Steinmetz, M. Selzer, B. Nestler, The parallel multi-physics phase-field framework PACE3D, Comput. Sci. 26 (2018) 1–12.
[36] M. Reder, D. Schneider, F. Wang, S. Daubner, B. Nestler, Phase-field formulation of a fictitious domain method for particulate flows interacting with complex and evolving geometries, Int. J. Numer. Methods Fluids (2021).
[37] T. Mittnacht, P.G.K. Amos, D. Schneider, B. Nestler, Morphological stability of three-dimensional cementite rods in polycrystalline system: A phase-field analysis, J. Mater. Sci. Technol. 77 (2021) 252–268.
[38] V.P. Laxmipathy, F. Wang, M.G. Selzer, B. Nestler, A two-dimensional phase–field study on dendritic growth competition under convective conditions, Comput. Mater. Sci. 186 (2021) 109964.
[39] R. Perumal, M. Selzer, B. Nestler, Concurrent grain growth and coarsening of two-phase microstructures; large scale phase-field study, Comput. Mater. Sci. 159 (2019) 160–176.
[40] S. Daniel, S. Ephraim, T. Oleg, R. Andreas, H. Christoph, Small strain multiphase-field model accounting for configurational forces and mechanical jump conditions, Comput. Mech. 61 (277-295) (2018).
[41] K.R. Satyanarayan, W. Eliasz, A.P. Miodownik, The effect of a magnetic field on the martensite transformation in steels, Acta Metall 16 (6) (1968) 877–887.
[42] M. Enomoto, H. Guo, Y. Tazuke, Y.R. Abe, M. Shimotomai, Influence of magnetic field on the kinetics of proeutectoid ferrite transformation in iron alloys, Metall. Mater. Trans. A 32 (3) (2001) 445–453.
[43] R. Fields, C.D. Graham, Effect of high magnetic fields on the martensite transformation, Metall. Trans. A 7A (1976) 719–721.
[44] Y. Mitsui, Y. Ikehara, K. Takahashi, S. Kimura, G. Miyamoto, T. Furuhara, K. Watanabe, K. Koyama, Fe-Fe3C binary phase diagram in high magnetic fields, J. Alloys Compd. 632 (2015) 251–255.

[45] C. Zhao, J. Li, Y. He, J. Wang, J. Wang, Effect of strong magnetic field on the microstructure and mechanical-magnetic properties of AlCoCrFeNi high-entropy alloy, J. Alloys Compd. 820 (2019).
[46] H.I. Faraoun, Y.D. Zhang, C. Esling, H. Aourag, Crystalline, electronic, and magnetic structures of O-Fe3C, x-Fe5C2, and n-Fe2C from first principle calculation, J. Appl. Phys. 99 (9) (2006) 093508.
[47] Y. Zhang, X. Zhao, N. Bozzolo, H.E. Changshu, L. Zuo, C. Esling, Low Temperature Tempering of a Medium Carbon Steel in High Magnetic Field, ISIJ Int 45 (6) (2005) 913–917.
[48] J.K. Choi, H. Ohtsuka, Y. Xu, W.Y. Choo, Effects of a Strong Magnetic Field on the Phase Stability of Plain Carbon Steels, Scripta Mater 43 (3) (2000) 221–226.